Available online at www.sciencedirect.com
ScienceDirect
Marine and Petroleum Geology 23 (2006) 893–900
Marine and Petroleum Geology
www.elsevier.com/locate/marpetgeo

Physical characterization of core samples recovered from Gulf of Mexico

Tae Sup Yun[a], Guillermo A. Narsilio[b], J. Carlos Santamarina[a,*]

[a]School of Civil and Environmental Engineering, Georgia Institute of Technology, 790 Atlantic Drive, Atlanta, GA 30332-0355, USA
[b]Department of Civil and Environmental Engineering, The University of Melbourne, Engineering Block D 321, Parkville, VIC 3010, Australia

Received 25 November 2005; received in revised form 21 August 2006; accepted 23 August 2006

Abstract

Seventy whole rounds from conventional cores obtained during drilling to ~300 mbsf at Atwater Valley and Keathley Canyon in the Gulf of Mexico in April and May 2005 were tested to determine geophysical and geomechanical parameters (liquid and plastic limit, porosity, specific surface, pH, sediment electrical conductivity, P- and S-wave velocities and undrained shear strength). Available data from a pressure core are included as well. Results show that the sediments are high specific surface plastic clays, and exhibit pronounced time-dependent stiffness recovery. Strains during coring disturb specimens, yet, the water content retains the effective stress history and permits gaining stiffness and strength information from conventional cores. Remolding is exacerbated when gas expands upon decompression; the limited pressure core data available show the advantages of preserving the pore fluid pressure during core recovery and testing. Valuable parameters for sediment characterization and engineering analysis are extracted from the data using pre-existing soil models.

Keywords: Gulf of Mexico; Sediments; Shear wave velocity; Stiffness; Strength; Electrical conductivity

1. Introduction

The Gulf of Mexico is a geological active and complex tectonic region. Sequences of sedimentary soils over buoyant salt deposits have lead to layering where deformational processes such as faulting and folding take place (Winker and Booth, 2000). The Gulf of Mexico sediments are rich in oil and gas and bear gas hydrates particularly near areas dominated by salt tectonics (Handa, 1990; Cooper and Hart, 2003; Francisca et al., 2005). Only few efforts have centered on the geotechnical characterization of shallow Gulf of Mexico sediments, and no sediment characterization has been done with preserved fluid-pressure specimens, in neither shallow nor deep sediments (Quiros et al., 1983; Silva et al., 2000; Young et al., 2000; Winters et al., 2002; Francisca et al., 2005). Yet, geotechnical properties are of critical importance for the analysis and design of seafloor processes and operations such as slope stability, borehole, anchors and foundations, hydraulic fracture and hydrate formation and destabilization.

The purpose of this paper is to present new geotechnical data gathered at two different sites in the Gulf of Mexico; Atwater Valley (Location AT #13: 27°56′59.6″N-latitude, 89°17′21.5″W-longitude. Locations ATM 1 and ATM 2: additional shallow coring <30 mbsf at mound) and Keathley Canyon (Location KC #151: 26°49′22.8″N-latitude, 92°59′12.1″W-longitude). Fig. 1 shows the location of both study sites. The water depth is 1291 m at AT #13 and 1322 m at KC #151. The AT #13 zone shows fluid/sediment intrusion and venting. All driling and coring operations were implemented onboard the semisubmersible vessel Uncle John (operated by CalDive International). The research cruise took place during April–May 2005. Sampling and test procedures, data, and interpretation are presented next.

*Corresponding author. Tel.: +1 404 894 7605; fax: +1 404 894 2281.
E-mail addresses: taesup@gatech.edu (T.S. Yun), narsilio@unimelb.edu.au (G.A. Narsilio), jcs@gatech.edu (J. Carlos Santamarina).

0264-8172/$ - see front matter © 2006 Elsevier Ltd. All rights reserved.
doi:10.1016/j.marpetgeo.2006.08.002

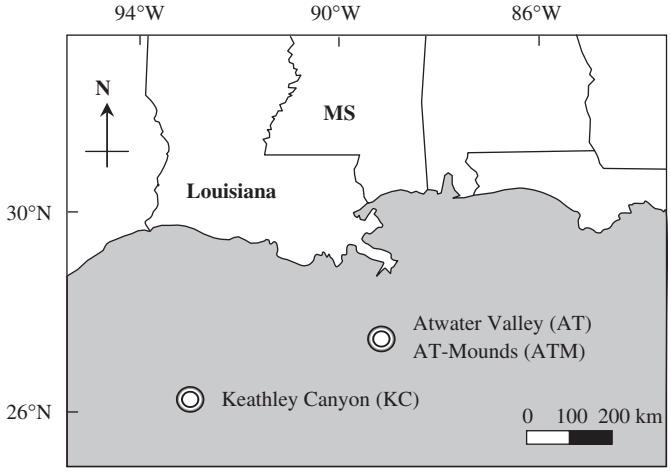

Fig. 1. Location of drilling sites—Gulf of Mexico: Atwater Valley, AT-mounds and Keathley Canyon.

2. Sampling and laboratory studies

Samples were gathered through conventional coring (Fugro pressure core FPC and Hyace rotary core HRC).

2.1. Conventional cores

The length of recovered cores varied between 5 and 9.5 m. It took approximately 1.5 h for the cores to be recovered from the seafloor to the initiation of core testing within a refrigerated laboratory on board. Voids developed within the sediment column due to gas expansion, typically in cores gathered at water depths in excess of ~1400 m; these voids could be seen through the transparent plastic core liner. A total of 70 whole round sections (0.05–0.1 m long) were tested as a part of this study to determine: gravimetric water content wc, liquid limit w_L and plastic limit w_P, pH, specific surface S_a, sediment electrical conductivity σ_{sed}, undrained shear strength S_u and elastic wave velocities V_p and V_s.

2.2. Pressure cores

Two pressure cores (KC-11P by FPC and KC-13R by HRC) were recovered at KC #151 and were tested under the preserved in situ fluid pressure of 14 MPa in both cases. Without releasing the pressure, these cores were transferred inside an instrumented high-pressure chamber to determine V_p, V_s, σ_{sed} and S_u. Chamber, instrumentation details and test results are documented in Yun et al. (2006).

2.3. Specimens and tests

Only a limited dataset is available from pressure cores. Therefore, most of the data reported herein were obtained from conventional cores. Properties measured in each case and test methods are summarized in Table 1.

Table 1
Sampling method, measured properties and devices

Properties	Devices	
	Non-pressure core	Pressure core[a]
Gravimetric water content (wc)[b]	Oven-dry (ASTM D2216)	—
Atterberg limits (w_L and w_P)[b]	Fall cone (ASTM D 4318)	—
Specific surface (S_a)[b]	Methylene blue adsorption	—
pH on sediment surface[c]	Non-bleeding pH strip ($\pm$0.25)	—
Thixotropy	Bender element (shear wave velocity)[d]	—
P-wave velocity (V_p)	Pinducer[e]	Pinducer
S-wave velocity (V_s)	Bender element[d]	Bender element
Undrained shear strength (S_u)	Laboratory calibrated penetrometer[f]	Strength probe
Electrical conductivity (σ)	Needle probe (Cho et al., 2004)	Needle probe

[a]Full details in Yun et al. (2006).
[b]On-shore measurements at Georgia Institute of Technology within 30 days after sampling.
[c]Freshly exposed surface.
[d]V_s using bender elements: coupled electrical-mechanical excitation of piezocrystal bimorph, at an operating frequency between 5 and 10 kHz.
[e]V_p using pinducer: frequency ~1.2 MHz, center contact pin diameter = 2 mm.
[f]Penetrometer: diameter = 6.35 mm, load to 3 tsf.

3. Results and analyses

3.1. Index properties

Fig. 2 shows measured index property profiles for data gathered at the two sites. The gravimetric water content wc and the sediment electrical conductivity σ_{sed} decrease with depth particularly in the upper 50 mbsf. High pH values in these sediments are often associated with the presence of carbonates (Francisca et al., 2005).

The specific surface S_a, i.e. the ratio between the grain surface area and their mass, is a good indicator of clay mineralogy. The specific surface measured for these sediments varies between $S_a \cong 62$ and 143 m^2/g (Table 2). High specific surface and platy particle geometry observed in scanning electron microscopy images suggest the presence of illite and/or montmorillonite (Mitchell and Soga, 2005). Laboratory experiments with synthetic hydrate demonstrate that the mechanical and electrical properties of hydrate bearing sediments depend on specific surface (Santamarina et al., 2005).

The liquid limit w_L and plastic limit w_P are procedurally defined water contents at the boundaries between slurry-to-plastic and plastic-to-non-plastic states. These limits are useful for the geo-mechanical classification of fine-grained sediments, as they reflect soil mineralogy and fluid-dependent soil fabric effects. The limits are obtained for selected specimens and are listed in Table 2. These values plot above the "A-line" on the plasticity chart,

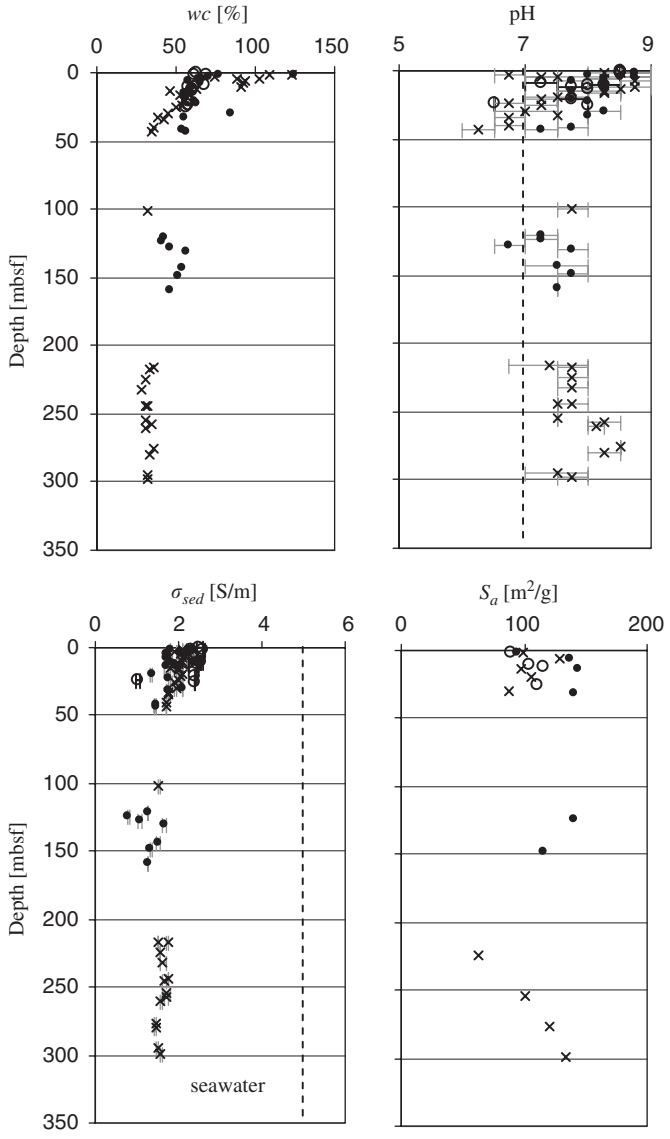

Fig. 2. Index property profiles from conventional cores—water content *wc*, pH, electrical conductivity of sediments σ_{sed}, and specific surface S_a. Symbols: filled circles AT #13; open circles ATM 1 and 2; crosses KC #151.

$I_P = 0.73(w_L - 22)$ where $I_p = (w_L - w_P)$; therefore, these soils are classified as inorganic clays of high plasticity, CH according to the Unified Soil Classification System (see Mitchell and Soga, 2005). The sediment at ATM 1 has a liquidity index $LI = (wc - w_P)/I_p = 0.977$ (close to one); specimens with $LI \geqslant 1$ are "sensitive" and lose strength upon remolding (Houston and Mitchell, 1969). The liquid limit w_L is in part a measure of specific surface S_a and empirical correlations have been identified, such as S_a $(m^2/g) = 1.8w_L - 34$ (Farrar and Coleman, 1967). Data in Table 2 confirm this correlation.

3.2. Mechanical properties

Fig. 3 shows measured V_p, V_s and S_u values with depth. The interpretation of these data follows.

3.2.1. Elastic wave velocities

The P-wave velocity V_p varies around the P-wave velocity of seawater $V_p \sim 1500$ m/s. Besides the potential effects of experimental difficulties, V_p values indicate the presence of free gas ($V_p < 1450$ m/s) or high shear stiffness in saturated sediments ($V_p > 1550$ m/s).

The shear wave velocity V_s is a measure of the soil skeletal stiffness and mass density. The skeletal shear stiffness is controlled by the effective mean stress σ'_m in the polarization plane. Therefore, the shear wave velocity is a power function of the effective stress acting on the sediment (Stokoe et al., 1992):

$$V_s = \alpha \left(\frac{\sigma'_m}{\text{kPa}} \right)^{\beta}, \tag{1}$$

where the α factor denotes the velocity of the sediment at $\sigma'_m = 1$ kPa and the β exponent captures the sensitivity of the soil stiffness to changes in effective stress. Typical values of the β-exponent are $\beta \cong 0$ for cemented soils, $\beta \cong 0.17$–0.25 for dense-to-loose sands and $\beta \geqslant 0.25$ for clayey soils. The value of β increases with the plasticity and porosity of clays and it is inversely related to the value of α as $\beta = 0.36 - \alpha$ (m/s)/700 (Santamarina et al., 2001). Data in Fig. 3 show $\beta \sim 0.3$, in agreement with the high plasticity, clayey nature of these sediments. (*Note*: the in situ mean stress on the polarization plane is estimated as $\sigma'_m = 0.75\sigma'_v$ presuming that the coefficient of earth pressure at rest is $K_0 \cong 0.5$; however, α and β parameters are not very sensitive to K_0.)

3.2.2. Undrained shear strength

The undrained shear strength S_u is the maximum shear resistance where sediments can mobilize when sheared under undrained conditions. The measured S_u increases with depth (Fig. 3). The dotted line corresponds to the empirical correlation between S_u and vertical effective stress σ'_v for normally consolidated clayey soils, $S_u = 0.22\sigma'_v$ (Mesri, 1989).

4. Discussion

4.1. Sediment compressibility

The sediment porosity is calculated from water content using gravimetric–volumetric relations. Assuming 100% saturation and mineral specific gravity $G_s = 2.65$, the sediment porosity is

$$n = \frac{G_s wc}{S + G_s wc}. \tag{2}$$

Fig. 4 shows the void ratio $e = n/(1-n)$ versus vertical effective stress σ'_v computed by integrating the depth-dependent sediment unit weight. The slope of the e-log(σ'_v/kPa) trend is the compression index C_c. Sediments at Keathly Canyon are significantly more compressible ($C_c = 0.735$) than sediments at Atwater Valley ($C_c = 0.292$). Compressibility is related to plasticity in clayey sediments (w_L or $I_p = w_L - w_P$) and many correlations have

Table 2
Core locations and characteristics

Core number[a]	Depth (mbsf)	wc (%)	w_L (%)	w_P (%)	S_a (m^2/g)	Core number	Depth (mbsf)	wc (%)	w_L (%)	w_P (%)	S_a (m^2/g)
Atwater Valley #13 site						*Keathley Canyon #151 site*					
AT13-1H-1	0.8	123.9				KC-1H-1	0.8	122.9			
AT13-1H-2	1.8	76.5			94.2	KC-1H-2	1.8	108.9			99.1
AT13-1H-3	2.8	70.4				KC-1H-3	2.8	74.5			
AT13-1H-4	3.8	67.3				KC-1H-4	3.8	102.8			
AT13-1H-5	4.8	64.3				KC-1H-5	4.8	88.1			
AT13-1H-6	5.8	57.2			137.0	KC-1H-6	5.8	93.1			128.4
AT13-2H-1	7.8	65.4				KC-1H-7	6.8	92.1			
AT13-2H-3	9.8	60.7				KC-2H-1	10.3	91.0			
AT13-2H-5	12.1	59.1				KC-2H-3	12.3	62.3			
AT13-2H-7	14.2	55.5	74.9	27.0	143.1	KC-2H-4	13.3	45.8			97.9
AT13-4H-2	20.1	61.5				KC-2H-5	14.3	57.8			
AT13-4H-5	22.5	63.1				KC-2H-6	15.3	57.6			
AT13-6H-1	29.2	84.5				KC-2H-7	16.2	52.2			
AT13-6H-4	32.2	54.6			140.7	KC-3H-1	19.4	54.7			105.2
AT13-8H-2	41.1	53.5				KC-3H-3	21.3	55.1			
AT13-8H-5	43.7	56.0				KC-3H-5	23.4	53.2	66.6	27.7	
AT13-9H-3	120.5	42.9				KC-3H-7	25.3	50.1			
AT13-9H-6	124.2	41.4			140.7	KC-4H-2	29.5	44.6			86.9
AT13-11H-3	127.6	46.7				KC-4H-5	32.5	38.8			
AT13-11H-4	130.8	55.9				KC-4H-7	34.5	42.2			
AT13-13H-2	142.9	53.5				KC-5H-3	40.0	36.0			
AT13-13H-5	148.3	51.7	77.0	30.5	115.0	KC-5H-6	43.0	34.9			
AT13-14H-1	158.6	46.0				KC-6C-3	102.0	32.5			
						KC-8C-2	216.5	35.8			
						KC-8C-3	217.5	33.8			
						KC-10C-2	224.8	30.3	51.2	20.7	62.4
ATM 1 and 2 sites						*KC-11P*	227	Pressure coring (FPC)			
ATM1-1H-1	0.8	69.5				KC-12C-2	231.8	28.1			
ATM1-1H-2	1.8	61.5			89.3	*KC-13R*	236	*Pressure coring (HRC)*			
ATM1-2H-2	8.2	68.3				KC-14C-2	243.8	32.2			
ATM1-2H-4	11.0	61.6				KC-14C-3	244.8	31.1			
ATM1-2H-6	12.5	60.6			115.0	KC-15C-3	254.8	31.1			100.3
ATM1-5H-2	20.7	57.2				KC-17H-2	257.8	34.1			
ATM1-5H-5	23.7	57.3				KC-17H-5	260.3	31.0			
ATM1-5H-7	25.7	57.0	57.8	23.1	111.3	KC-19H-2	276.2	36.1			119.9
ATM2-1H-1	0.7	62.8				KC-19H-6	280.2	32.7			
ATM2-2H-4	11.1	57.2			104.0	KC-20H-2	294.5	31.8			
ATM2-2H-5	12.7	59.8				KC-20H-6	298.5	31.6			133.3

[a]The number after the dash indicates the recovered core number followed by the coring method (H: Fugro Hydraulic Piston Corer, C: Fugro Corer). The last number represents the successive round sections in the given core.

been suggested for engineering practice (Kulhawy and Mayne, 1990; Terzaghi et al., 1996). The computed C_c values are in general agreement with those empirical trends.

The critical state parameter λ is the slope of the critical state line when projected onto the e-ln(p'/kPa) space, where p' is the mean effective stress. The value of λ is related to the compression index C_c as $\lambda = C_c/2.303$ (Wood, 1990); then, the estimated values of λ for these sediments are $\lambda = 0.127$ (AT) and $\lambda = 0.319$ (KC). These results suggest that important compression and critical state strength parameters can be inferred from porosity variation with depth under the quasi-homogeneous sediment assumption.

4.2. Porosity and electrical conductivity

The electrical conductivity of the pore fluid σ_{pf} is computed from salinity measurements gathered by researchers from Scripps Institution of Oceanography during the cruise (M. Kastner, personal communication, 2005). The assumed linear relation between salinity and pore fluid (electrolyte) conductivity is $\sigma_{pf} = 0.15 \cdot \text{Salinity}$ (Annan, 1992). This conversion is verified by testing pore fluid extracted from sediments using a conductivity-meter (AR50, Fisher-Scientific).

The sediment electrical conductivity σ_{sed} combines pore fluid conductivity, porosity and surface conduction (Santamarina et al., 2001). Disregarding the effect of surface conduction (proper in marine sediments), the sediment electrical conductivity σ_{sed} and the pore fluid conductivity σ_{pf} are related through the porosity n as given by Archie's law (Archie, 1942). In the simplest form, a one-unknown version of Archie's law is

$$\sigma_{sed} = An\sigma_{pf}, \tag{3}$$

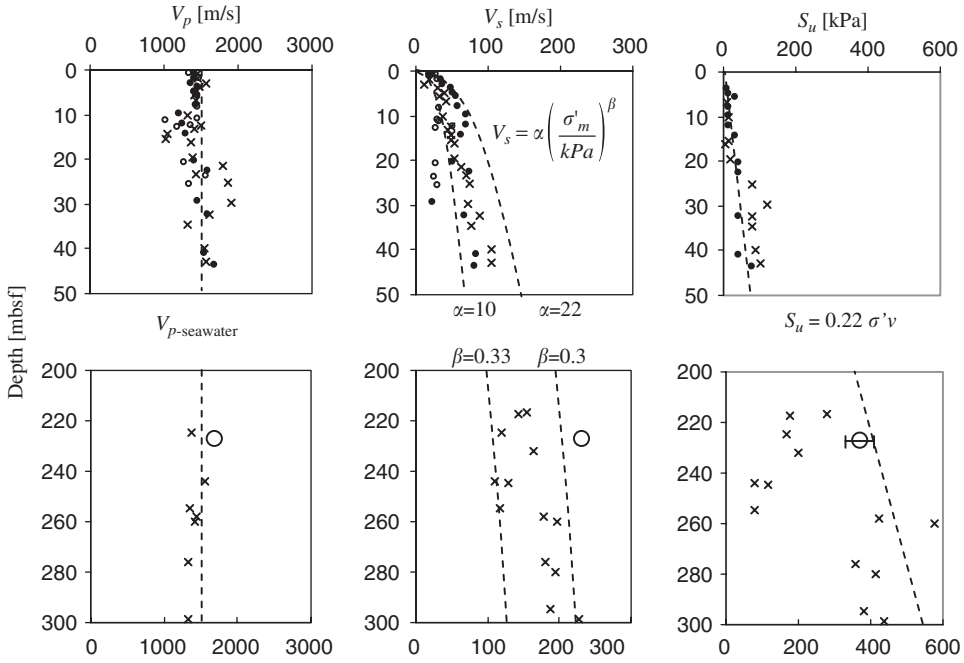

Fig. 3. Elastic wave velocities and undrained shear strength with depth. Symbols: filled circles AT #13; open circles ATM 1 and 2; crosses KC #151. The dotted line in the S_u profile corresponds to the empirical correlation between undrained shear strength and effective vertical stress. The big open circles at ~227 mbsf represent values gathered from the pressure core at KC-11P.

where A is a fitting parameter. Fig. 5a shows the plot of σ_{sed} versus $n\sigma_{pf}$. Eq. (3) fits the data with $A = 0.5$ (typically, an exponent $m > 1$ is imposed to porosity n in Eq. (3), so higher A values are reported in the literature).

4.3. Water content and undrained shear strength

The effective confining stress determines both the strength and the porosity of fine-grained clayey sediments. Therefore, water content wc and the undrained shear strength S_u are expected to be correlated. This is depicted in Fig. 5b. Prior studies show that water content is related to shear strength as (Sridharan and Prakash, 1999; Koumoto and Houlsby, 2001)

$$S_u = 1.4 \times 10^7 wc^{-\delta}(\text{kPa}), \tag{4}$$

where the exponent δ is associated to the plasticity index. The fitted value for these sediments is $\delta = 3.21$ and it is consistent with values found by previous researchers for similar plasticity clays (Sridharan and Prakash, 1999; Koumoto and Houlsby, 2001; Whittle and Sutaburt, 2005).

The strength of the deeper sediments ($z > 50$ mbsf) is lower than predicted for undisturbed specimens (as compared to $S_u = 0.22\sigma'_v$ in Fig. 3). This deviation suggests that these specimens have experienced significant disturbance during sampling, however, a definitive conclusion is premature due to the inherent uncertainty in such correlations.

4.4. Undrained shear strength (large-strain) and shear wave velocity (small-strain)

The effective stress determines not only the undrained shear strength $S_u = 0.22\sigma'_v$ (Fig. 3), but the skeletal shear stiffness as well, in this case in terms of $V_s = \alpha(\sigma'_v/\text{kPa})^{\beta}$ (Eq. (1)–Fig. 3). Therefore, the following stiffness–strength correlation is anticipated from these expressions:

$$V_s = \alpha 4.55^{\beta}\left[\frac{S_u}{\text{kPa}}\right]^{\beta} = 19.4\frac{\text{m}}{\text{s}}\left[\frac{S_u}{\text{kPa}}\right]^{0.36}. \tag{5}$$

Data and the trend predicted with this equation are shown in Fig. 5c. It is important to highlight that while small and large strain phenomena involve very different particle-level processes and are not causally related, they are correlated through their control variable σ'_v.

4.5. Mechanical properties from unconfined specimens

Can a stress-dependent stiffness be determined from unconfined samples? The porosity of uncemented high-plasticity soils is strongly related to the maximum effective confining stress that these sediments have experienced. In turn, interparticle coordination depends on porosity, and controls stiffness. Therefore, the water content in saturated specimens preserves the effect of effective confining stress on stiffness (Klein and Santamarina, 2005). This observation can be extended to the stress-dependent undrained strength S_u, however, the analysis must include the development of dilation and suction during shear.

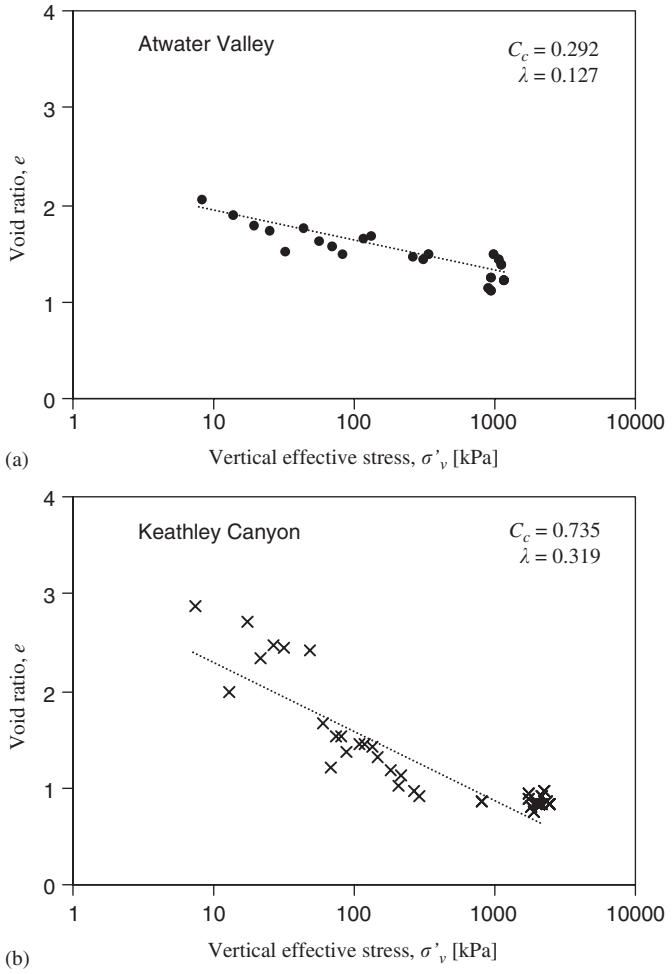

Fig. 4. Compressibility—*Note*: void ratio e is related to porosity n as $e = n/(1-n)$.

Conversely, diagenetic cementation and gas dissolution/expansion hinder the assessment of in situ properties from recovered specimens. These observations suggest that while water content retains the memory of the effective stress history, mechanical parameters measured on unconfined specimens should be considered as indicators of the true values.

4.6. Thixotropy

Thixotropy is an isothermal time dependent process that occurs at constant volume and without change in material composition (Mitchell, 1960; Mitchell and Soga, 2005). Montmorillonitic sediments are particularly prone to exhibit thixotropic behavior. The thixotropic recovery of stiffness in sediments from both sites is studied by thoroughly remolding specimens and monitoring the evolution of shear wave velocity without moisture loss (no suction generation). Fig. 6 shows that the shear wave velocity in specimens from the two sites increases with time towards the undisturbed value. Similar stiffness (and strength) recovery is observed in other high specific surface soils, Mexico City clayey sediments (see for example

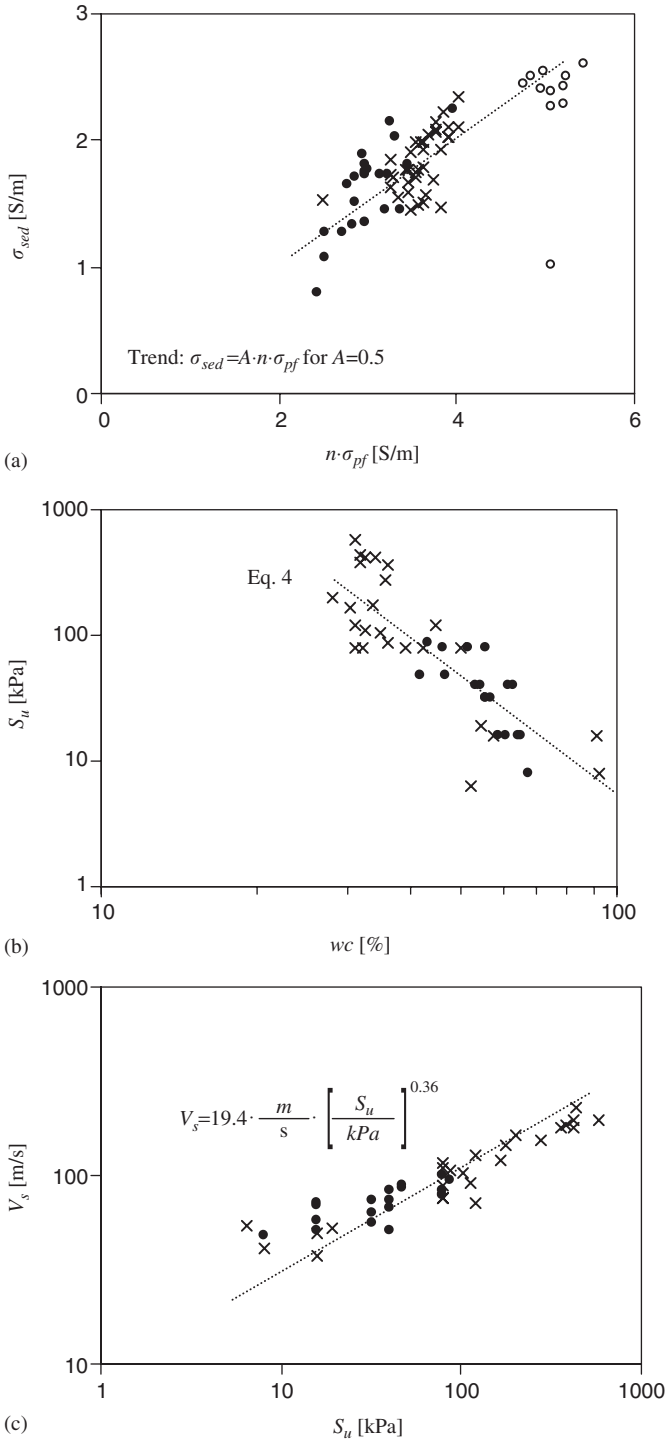

Fig. 5. Parameter correlations. Symbols: filled circles AT #13; open circles ATM 1 and 2; crosses KC #151. *Note*: σ_{pf} computed from salinity measurements conducted by Scripps researchers (M. Kastner, personal communication, 2005).

data in Díaz-Rodríguez and López-Flores, 1999; Díaz-Rodríguez and Santamarina, 1999).

4.7. Implications from pressure core measurements

Data gathered from conventional cores are compared against the limited pressure data available from this cruise

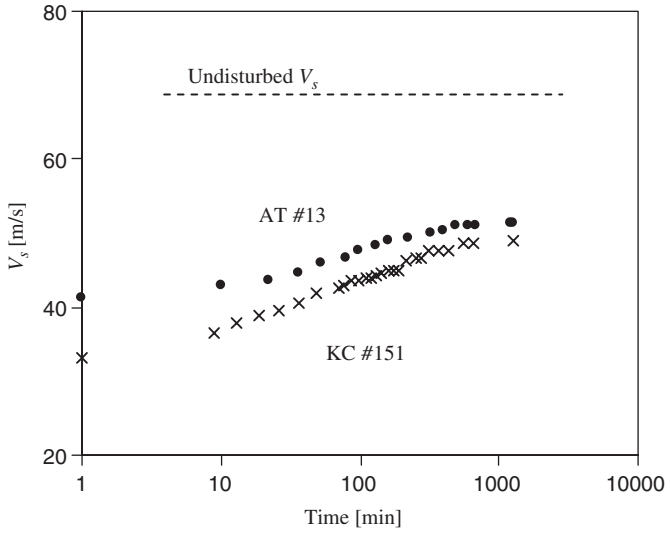

Fig. 6. Time-dependent stiffness recovery. Evolution of shear wave velocity with time.

(large open circles in Fig. 3). S-wave velocity and strength data from the pressure core hint to the importance of maintaining the fluid pressure constant, even when effective stress is drastically reduced. Apparently, gas expansion during depressurization disturbs the sediment and causes extensive remolding, reducing the measured shear wave velocity of conventional core specimens. The undrained shear strength results lead to similar conclusions. Measurements on more pressure cores are needed to further confirm this observation and it is the subject of future expeditions. Sampling effects (coring-induced strains, change in effective stress, and gas dissolution and expansion) are exacerbated in sensitive sediments such as those encountered here.

5. Conclusions

Sediments encountered in the study area are classified as inorganic clays of high plasticity, have high specific surface, and exhibit pronounced time-dependent stiffness recovery.

Strains during coring and sampling cause partial disturbance in recovered specimens. The water content retains the effective stress history of these plastic sediments and permits assessing stiffness and strength from cores (assuming no diagenetic effects).

Remolding is exacerbated when dissolved gas comes out of solution and expands upon decompression. Limited data suggest that the recovery of pressure cores followed by stiffness and strength testing under pressure are advantageous when hydrate or just gas is present in the sediment.

Data analysis in the context of pre-existing soil models permits extracting parameters that link pore fluid conductivity to sediment conductivity (Archie's law), stress history to porosity (critical state theory), and stress-dependent small-strain stiffness (Hertzian type) to stress-dependent large-strain strength (Coulomb-type).

Acknowledgments

This research was conducted at Georgia Tech with support provided by the Joint Industry Project for Methane Hydrate, administered by ChevronTexaco with funding from award DE-FC26-01NT41330 from DOE's National Energy Technology Laboratory. Additional support was provided by the Goizueta Foundation.

References

Annan, A.P., 1992. Ground Penetrating Radar: Workshop Notes, Sensors and Software. Mississauga, Ontario, Canada.

Archie, G.E., 1942. The electrical resistivity log as an aid in determining some reservoir characteristics. Trans. Am. Inst. Min. Metall. Pet. Eng. 146, 54–62.

Cho, G.C., Lee, J.-S., Santamarina, J.C., 2004. Spatial variability in soils: high resolution assessment with electrical needle probe. J. Geotech. Geoenviron. 130 (8), 843–850.

Cooper, A.K., Hart, P.E., 2003. High-resolution seismic-reflection investigation of the northern Gulf of Mexico gas-hydrate-stability zone. Mar. Petrol. Geol. 19, 1275–1293.

Díaz-Rodríguez, J.A., López-Flores, L., 1999. Study of microsstructure using resonant column testing. Earthquake Geotech. Eng. Rotterdam, pp. 89–94.

Díaz-Rodríguez, J.A., Santamarina, J.C., 1999. Thixotropy: the case of Mexico City coils, XI Panamerican Conference on Soil Mechanics and Geotechnical Engineering. Iguazu Falls: Brazil. pp. 441–448

Farrar, D.M., Coleman, J.D., 1967. The correlation of surface area with other properties of nineteen British clays. J. Soil Sci. 18 (1), 118–124.

Francisca, F.M., Yun, T.S., Ruppel, C., Santamarina, J.C., 2005. Geophysical and geotechnical properties of near-surface sediments in the Northern Gulf of Mexico gas hydrate province. Earth Planet. Sci. Lett. 237, 924–939.

Handa, Y.P., 1990. Effect of hydrostatic pressure and salinity on the stability of gas hydrates. J. Phys. Chem. 94, 2652–2657.

Houston, W.N., Mitchell, J.K., 1969. Property interrelationships in sensitive clays. Am. Soc. Civil Eng. J. Soil Mech. Found. Div. 95 (SM4), 1037–1062.

Klein, K.A., Santamarina, J.C., 2005. Behavior of very soft sediments: wave-based monitoring. Int. J. Geomech. 5 (2), 147–157.

Koumoto, T., Houlsby, G.T., 2001. Theory and practice of the fall cone test. Geotechnique 51 (8), 701–712.

Kulhawy, F.H., Mayne, P.W., 1990. Manual on estimating soil properties for foundation design, Report No. El-6800. Electric Power Research Institute, p. 306.

Mesri, G., 1989. Re-evaluation of $S_u = 0.22\ \sigma'_p$ using laboratory shear tests. Can. Geotech J. 26 (1), 162–164.

Mitchell, J.K., 1960. Fundamental aspects of thixotropy in soils. J. Soil Mech. Found. Div. 86 (SM3), 19–52.

Mitchell, J.K., Soga, K., 2005. Fundamentals of Soil Behavior, third ed. Wiley, New York.

Quiros, G.W., Young, A.G., Pelletier, J.H., Chan, J.H.-C., 1983. Shear strength interpretation for Gulf of Mexico clays. Geotech. Practice Offshore Eng. ASCE Conference, pp. 144–165.

Santamarina, J.C., Klein, K.A., Fam, M.A., 2001. Soils and Waves. Wiley, New York.

Santamarina, J.C., Yun, T.S., Lee, J.Y., Martin, A., Francisca, F.M., Ruppel, C., 2005. Mechanical, Thermal and Electromagnetic Properties of Hydrate-bearing clay, Silt, and Sand at Various Confining Pressure. American Geophysical Union, San Francisco, CA, USA.

Silva, A., Baxter, C., Bryant, W., Bradshaw, A., LaRosa, A.P., 2000. Stress–strain behavior and stress state of Gulf of Mexico clays in relation to slope processes. Proceedings of Offshore Technology Conference, May1–4, Houston: TX, USA. pp. 451–460

Sridharan, A., Prakash, K., 1999. Mechanisms controlling the undrained shear strength behavior of clays. Can. Geotech. J. 36, 1030–1038.

Stokoe, K. H., Lee, J. N. K., Lee, S. H. H., 1992. Characterization of Soil in Calibration Chambers With Seismic Waves. Potsdam, NY, USA, p. 363.

Terzaghi, K., Peck, R.B., Mesri, G., 1996. Soil Mechanics In Engineering Practice, third ed. Wiley, New York.

Whittle, A.J., Sutaburt, T., 2005. Parameters for Average Gulf Clay and Prediction of Pile Set-up In The Gulf of Mexico, Geotechnical special publication No. 128: Soil Constitutive Models: Evaluation, Selection, and Calibration, Reston, VA, pp. 440–458.

Winker, C. D., Booth, J.R., 2000. Sedimentary dynamics of the salt-dominated continental slope, Gulf of Mexico: Integration of observations from the seafloor, near-surface and deep subsurface. In: GCSSEPM Foundation 20th Annual Research Conference of, Deep-Water Reservoirs of the World, New Orleans, LA, pp. 1059–1086.

Winters, W.J., Nouosel, I., Boldina, O.M., Waite, W.F., Lorenson, T.D., Paull, C.K., Bryant, W., 2002. Physical properties of sediment related to gas hydrate in the northern Gulf of Mexico. EOS Trans. Am. Geophys. Union Fall Meet., 83, F1388 (abstract T22B-1144).

Wood, D.M., 1990. Soil Behaviour and Critical State Soil Mechanics. Cambridge University Press, New York.

Young, A.G., Honganen, C.D., Silva, A.J., Bryant, W.R., 2000. Comparison of geotechnical properties of large-diameter long cores and borings in deep water Gulf of Mexico. Proceeding of the Offshore Technology Conference, May1–4, Houston: TX, USA. pp. 427–438

Yun, T.S., Narsilio, G.A., Santamarina, J.C., Ruppel, C., 2006. Instrumented pressure testing chamber for characterizing sediment cores recovered at in-situ hydrostatic pressure. Mar. Geol. 229 (3–4), 285–293.